Wettability of AFM Tip Influences the Profile of Interfacial Nanobubbles

Teshima, Hideaki
Department of Aeronautics and Astronautics, Kyushu University

Takahashi, Koji
Department of Aeronautics and Astronautics, Kyushu University

Takata, Yasuyuki
International Institute for Carbon-Neutral Energy Research (WPI-I2CNER), Kyushu University

Nishiyama, Takashi
Department of Mechanical Engineering, Fukuoka University

出版情報：Journal of Applied Physics. 123 (5), pp.054303-, 2018-02-02. American Institute of Physics : AIP
バージョン：

Wettability of AFM tip influences the profile of interfacial nanobubbles

Cite as: J. Appl. Phys. **123**, 054303 (2018); https://doi.org/10.1063/1.5010131
Submitted: 23 October 2017 • Accepted: 18 January 2018 • Published Online: 02 February 2018

Hideaki Teshima, Koji Takahashi, Yasuyuki Takata, et al.

Wettability of AFM tip influences the profile of interfacial nanobubbles

Hideaki Teshima,[1,2] Koji Takahashi,[1,2,a)] Yasuyuki Takata,[2,3] and Takashi Nishiyama[4]
[1]*Department of Aeronautics and Astronautics, Kyushu University, Nishi-Ku, Motooka 744, Fukuoka 819-0395, Japan*
[2]*International Institute for Carbon-Neutral Energy Research (WPI-I2CNER), Kyushu University, Nishi-Ku, Motooka 744, Fukuoka 819-0395, Japan*
[3]*Department of Mechanical Engineering, Kyushu University, Nishi-Ku, Motooka 744, Fukuoka 819-0395, Japan*
[4]*Department of Mechanical Engineering, Fukuoka University, Jonan-Ku, Nanakuma 8-19-1, Fukuoka 814-0180, Japan*

(Received 23 October 2017; accepted 18 January 2018; published online 2 February 2018)

To accurately characterize the shape of interfacial nanobubbles using atomic force microscopy (AFM), we investigated the effect of wettability of the AFM tip while operating in the peak force tapping (PFT) mode. The AFM tips were made hydrophobic and hydrophilic by Teflon AF coating and oxygen plasma treatment, respectively. It was found that the measured base radius of nanobubbles differed between AFM height images and adhesion images, and that this difference depended on the tip wettability. The force curves obtained during the measurements were also different depending on the wettability, especially in the range of the tip/nanobubble interaction and in the magnitude of the maximum attractive force in the retraction period. The difference suggests that hydrophobic tips penetrate the gas/liquid interface of the nanobubbles, with the three phase contact line being pinned on the tip surface; hydrophilic tips on the other hand do not penetrate the interface. We then quantitatively estimated the pinning position and recalculated the true profiles of the nanobubbles by comparing the height images and adhesion images. As the AFM tip was made more hydrophilic, the penetration depth decreased and eventually approached zero. This result suggests that the PFT measurement using a hydrophilic tip is vital for the acquisition of reliable nanobubble profiles. *Published by AIP Publishing*. https://doi.org/10.1063/1.5010131

INTRODUCTION

Nanoscale bubbles at solid/liquid interfaces are attracting increased attention because of their applications in several areas of engineering, including reduction of surface drag on fluid flow,[1] cleaning of nanopatterned surfaces,[2] boiling with low superheat,[3] and wafer-scale transfer of graphene films.[4] These applications are closely related with the unique properties of nanobubbles, such as significantly higher contact angles than those observed on the macroscale[5–19] and a surprisingly long lifetime,[20–23] which contradicts the classical thermodynamic prediction that a nanoscale bubble should dissolve within a few hundred microseconds.[24,25] To explain these counterintuitive properties, many theories have been proposed.[26–35] Some studies have suggested that the contact angle is increased by the line tension, which results from an imbalance of the intermolecular force along the base curvature of the nanobubbles.[33,34] Another theory holds that nanobubbles are stabilized because the gas outflux resulting from the high Laplace pressure and the gas influx at the three-phase contact line are in equilibrium.[27,28,35] These theories can explain some of the experimental results; however, a complete explanation has not been achieved. To apply interfacial nanobubbles in engineering fields, further understanding of their properties based on observation data is needed. So far, several experimental methods have been developed to observe interfacial nanobubbles with sufficient spatial resolution, such as liquid cell microscopy,[36–38] total internal reflection fluorescence microscopy,[39,40] and atomic force microscopy (AFM).[5–18,20–23,41–43] Above all, AFM imaging is the most preferred because of the ability to collect three-dimensional profiles with nanometer-scale resolution. Therefore, almost all existing theories are based on topographical data obtained using AFM. To confirm and enhance the reliability of the nanobubble theories, the accuracy of the AFM data is important. In some recently reported studies, nanobubble profiles have been corrected by taking the broadening of the AFM tip into consideration[10,11] and by estimating the undisturbed shapes of the bubbles through an extrapolation of the applied force to zero.[13,44,45] In addition, the influence of AFM tip wettability on the gas phase measurement should be considered; this effect may be equal to or greater than the effect of tip shape. However, experimental results regarding the influence of AFM tip wettability on the interfacial nanobubbles have been reported only by Schönherr's group, in which the interactions between hydrophilic and hydrophobic AFM tips and argon nanobubbles were analyzed using a combination of tapping mode and force volume mode.[44,45] Recently, it was reported that the base radii of nanobubbles visible in AFM height images are slightly smaller than those derived from adhesion images, leading to underestimation of the nanobubble profiles.[13] This implies that the nanobubbles cannot be seen in height images if they are too small. It has also been reported that the

[a)]Author to whom correspondence should be addressed: takahashi@aero.kyushu-u.ac.jp

wettability and structure of the substrate surface affect the stability, generation position, and shape of the nanobubbles.[18,19,23,46,47] For better understanding of the influence of substrate surface on the nanobubbles, and for future applications such as the precise control of the position and size of the generated nanobubbles, it is necessary to detect the nanobubbles at small size extremes. Therefore, it is essential to establish the cause(s) of the underestimation and to employ experimental conditions to avoid such underestimation. In the present study, we prepared hydrophobic, hydrophilic, and unprocessed (intermediate wettability) AFM tips and measured the nanobubbles formed at the interface of highly ordered pyrolytic graphite (HOPG) and pure water, using the peak force tapping (PFT) mode. The details of the PFT mode are described in the "Methods" section. Simultaneous with the height images, adhesion images and force curves were also acquired using peak force quantitative nanomechanical mapping (PF-QNM). We compared the obtained images and force curves to gain insights into the influence of AFM tip wettability on the measured profile of interfacial nanobubbles.

METHODS

AFM probes with three levels of wettability were prepared by processing the surfaces of a ScanAsyst-Fluid+ cantilever (tip radius: 2–12 nm; spring constant: 0.7 N m^{-1}). This probe has a silicon tip and low spring constant, making it suitable to measure interfacial nanobubbles in the PFT mode. The wettability of the tips was assumed to be the same as the wettability of similarly processed silicon wafer surfaces (i.e., reference surfaces). Therefore, we evaluated the wettability of three types of tip surfaces by measuring the water contact angle on the reference surfaces using the sessile drop method. The unprocessed tip is considered to have a native oxide thin film, and thus a silicon surface with a native oxide thin film was used as a reference surface. The tip was made hydrophilic by oxygen plasma treatment (Plasma Reactor 500, Yamato, Japan) for 30 min, where the power and flow rate were set to 150 W and 70 sccm, respectively; the treated tip was then left for 24 h in a sealed case. The silicon surface treated in the same way was used as a reference surface. The hydrophobic tip was prepared by coating it with a thin film of Teflon AF (DuPont Inc., Wilmington, DE, USA); we used a Teflon-coated silicon surface as a reference surface. The Teflon AF was dissolved in Fluorinert FC-770 liquid (3M Company, St. Paul, MN, USA) to form a 0.2 wt. % solution, which was applied dropwise to the tip. To form a thin film, the tip was then baked at 95 °C for 1 h. The thickness of the Teflon film fabricated in a similar fashion on a silicon surface was 50 nm. We confirmed that the Teflon film was smoothly fabricated on the tip surface (see Fig. S1). The contact angles of the hydrophilic, unprocessed, and hydrophobic reference surfaces were approximately 15°, 70°, and 120°, respectively. Therefore, it can be considered that the functionalization made a difference in the wettability of the tip surfaces. The spring constants of the three probes were calibrated in water using a thermal tuning method before the measurements.

The nanobubbles were generated at the interface between HOPG (SPI-1 grade, 10 mm × 10 mm, Alliance Biosystems, Inc., Japan) and pure water by the solvent exchange method.[5,8,16,22,23,39–41,46,48–52] Pure water was prepared using a water purifier (RFP742HA, Advantec, Japan) without degassing. An HOPG with a thickness of ∼0.5 mm was fixed on a stainless-steel Petri dish and immersed in ethanol for several minutes. The ethanol was then exchanged by adding pure water. Ethanol has a higher air solubility than pure water. Therefore, this process creates a local air-supersaturated condition at the HOPG/pure water interface, resulting in the formation of interfacial nanobubbles. Clean disposable pipettes were used to add the ethanol and pure water to avoid contamination.[53]

The measurements were conducted using the PFT mode of a Dimension Icon AFM system (Bruker AXS). The PFT mode has two advantages. First, more accurate height images can be obtained compared with the normal AFM tapping mode because the cantilever operates at a lower frequency than its resonance frequency and receives feedback from all turnaround points (i.e., points where the applied repulsive force becomes identical with a set value). Conventional tapping mode operation cannot receive feedback from all turnaround points because the cantilever oscillates at its resonance frequency. Second, by plotting the forces applied to the cantilever on the vertical axis versus the tip-to-sample distance (i.e., separation) on the horizontal axis, the force curve can be obtained during the imaging. By comparing the force curves measured on the interfacial nanobubbles using tips with different wettability, the interaction between the tips and the nanobubbles can be revealed. In addition, adhesion images based on the force curves can be obtained, which are composed of the maximum values of the attractive force in the retraction period, allowing one to sensitively visualize the existence of nanoscale gas phases. The height and adhesion data were captured with a resolution of 256 × 256 pixel and a scan rate of 0.5 Hz. The velocity of the tip approach was 800 μm/s in all measurements. Raw deflection error versus Z piezo position curves were modified into force versus separation curves. The deflection error was recalculated into an applied force by using the calibrated cantilever stiffness. The Z piezo position was also recalculated into the separation, which represented the distance between the tip and turnaround points. Thus, the force versus separation curve represents the relationship between the force and vertical position of the tip end above the turnaround point.

RESULTS AND DISCUSSION

The height and adhesion images of the interface between the HOPG and pure water scanned by AFM tips with different wettability are shown in Fig. 1. In all images, semispherical shape objects were observed. To distinguish the nanobubbles from the contaminant nanodroplets, previous studies have used several methods, such as degassing,[53] force volume measurement,[15] combined AFM and optical methods,[54,55] and strong peak force setpoint scanning.[17] In this study, we employed the method of An *et al.*[17] and confirmed that the semispherical shape objects were interfacial nanobubbles. The details are described in the supplementary material (see Fig. S2). The nanobubbles were also observed

at the same positions in the adhesion images. The base shapes of the nanobubbles were observed to differ between Figs. 1(a) and 1(b), both imaged using the hydrophobic tip. In addition, the base areas of the nanobubbles shown in Fig. 1(a) were either smaller than those in Fig. 1(b), or completely invisible. This implies that the heights of the nanobubbles were not accurately detected because the hydrophobic tip had reached the HOPG surface before receiving effective feedback at the nanobubble surfaces. The base shapes of the nanobubbles in Fig. 1(c) were similar to those in Fig. 1(d). However, as done for the images scanned by the hydrophobic tip, the base radii of the nanobubbles in the height image in Fig. 1(c) were underestimated compared with those from the adhesion image in Fig. 1(d). The base radii of the nanobubbles, shown in Figs. 1(e) and 1(f), indicate that those of the height image and the adhesion image were comparable when scanned with the hydrophilic tip.

The force curves measured by the AFM tips with different wettability are shown in Fig. 2. They were obtained above the center of nanobubbles having nearly the same base

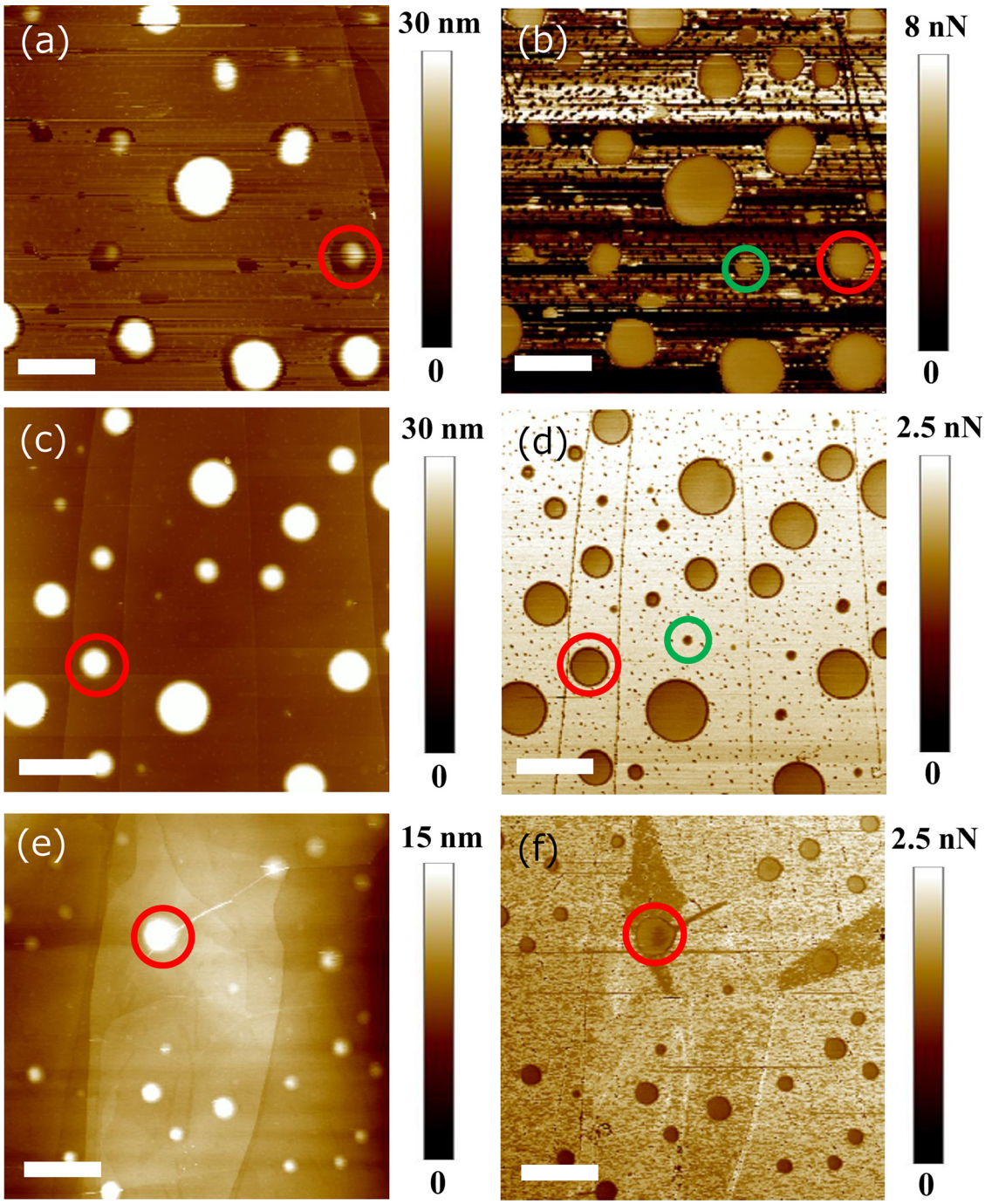

FIG. 1. AFM images ($5 \times 5\ \mu$m) of the interfacial nanobubbles scanned using [(a) and (b)] hydrophobic, [(c) and (d)] unprocessed, and [(e) and (f)] hydrophilic tips. The height images [(a), (c), and (e)] and adhesion images [(b), (d), and (f)] were acquired at the same time, respectively. The peak force setpoint was constant at 300 pN in all experiments. The scale bar is 1 μm. The red circles indicate the nanobubbles on which the force curves were measured. The green circles indicate the nanobubbles which can be seen in the adhesion images only.

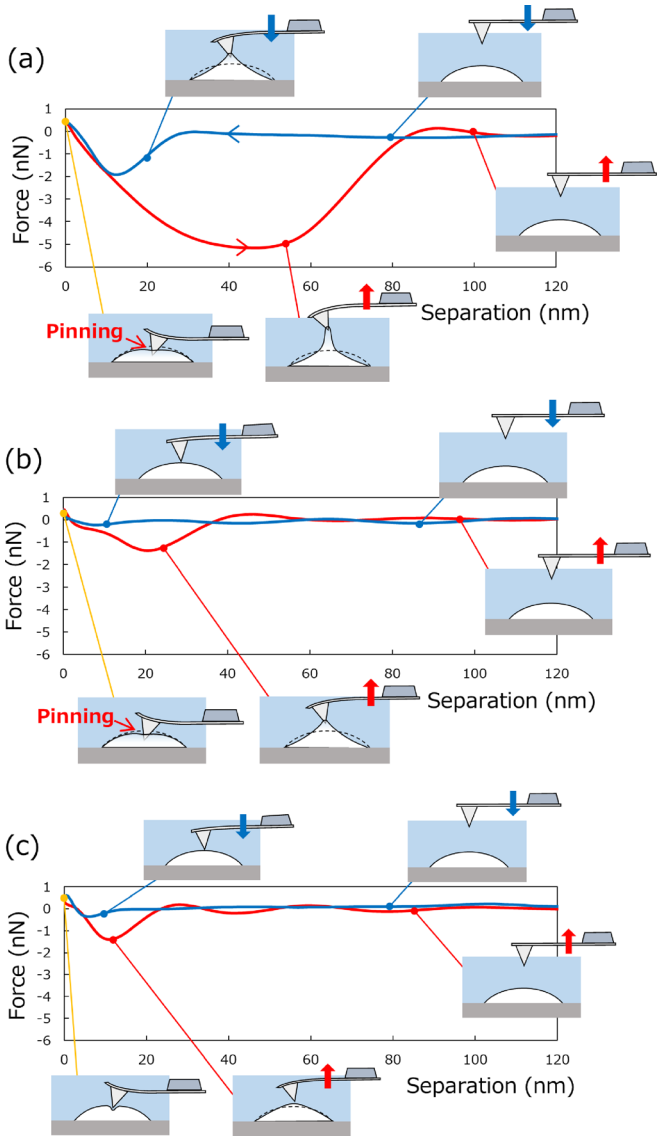

FIG. 2. Force curves between interfacial nanobubbles and (a) hydrophobic, (b) unprocessed, and (c) hydrophilic AFM tips. The blue curve and red curve indicate the force curves in the approach and retraction, respectively. The interactions between the nanobubbles and the tips are drawn in the insets. The hydrophobic and unprocessed tips penetrate the gas/liquid interface and experience repulsive and attractive forces owing to the pinning of the three-phase contact line at the tip surfaces. In contrast, the hydrophilic tip does not penetrate the interface and experiences the forces through the thin liquid film between the tip and the nanobubbles.

radius in the adhesion images, indicated by the red circles shown in Fig. 1. The positive and negative values of the curve correspond to the repulsive and attractive forces applied to the tip, respectively. The zero point of the horizontal axis refers to the turnaround point where the repulsive force reached 300 pN of the peak force setpoint. The separation refers to the distance from the turnaround point to the AFM tip position. The force curves differ from each other, such as at the onset and the end points of the tip/nanobubble interaction (jump-in and jump-out points as described below); the magnitude of the maximum attractive force in the retraction was also different using different AFM tips.

As shown by the force curve obtained by the hydrophobic AFM tip [Fig. 2(a)], the interaction between the tip and the nanobubble was the strongest and of the longest duration in the approach period. The tip started to experience an attractive force at a separation distance of approximately 30 nm and the force reached a maximum at a separation of 12 nm in the approach. This jump-in at 30 nm is derived from the negative meniscus formed at the surface of the tip, which means that the nanobubble locally protrudes. It has been reported that the nanobubble interface deformed in the direction of the tip before attaching.[44,45] The Teflon-coated AFM tip used in this experiment probably has higher hydrophobicity than that used in the previous report. Therefore, the phenomenon of the gas/liquid interface jump should occur in this approach. As the tip approached the interface at a separation range shorter than 12 nm, the attractive force gradually decreased and eventually turned into a repulsive force. We attribute this repulsive force to pinning resulting from the surface chemical- and geometrical heterogeneities of the AFM tip. The negative meniscus is changed to positive (i.e., the nanobubble is locally depressed) as the AFM tip advances downward because the three-phase contact line is pinned, so that the attractive force originating from the meniscus also becomes repulsive. If the hydrophobic tip is ideally smooth, the gas/liquid interface will not be pinned and will continue to dry on the surface, and the repulsive force therefore will not occur. A simulation conducted by Zhang *et al.*[56] showed that the repulsive force is not found in the force curve when the surface of the hydrophobic tip is ideally smooth, which supports our assumption. In the retraction, the attractive force continued to increase up to a separation distance of 50 nm (jump-out point) and reached approximately 5 nN. This is because strong pinning at the tip surface induces a substantial deformation of the nanobubble gas/liquid interface. After passing the jump-out point in the retraction, the gas/liquid interface was unpinned from the tip surface and then the force returned to zero.

The force curve measured by the unprocessed AFM tip is shown in Fig. 2(b). In the approach of this force curve, the attractive force experienced by the tip was weaker than that of the hydrophobic tip. In addition, the attractive force started to appear at a separation distance of 10 nm. This result suggests that the jump of the gas/liquid interface toward the tip surface was small or hardly occurred because the hydrophobicity of the unprocessed tip was lower than that of the hydrophobic tip. After the gas/liquid interface and the tip were in contact, the tip penetrated the interface and experienced a repulsive force through the above-mentioned pinning mechanism. The attractive force in the retraction was also weaker and of shorter duration than that in the force curve of the hydrophobic tip. This is because the three-phase contact line formed at the surface of the unprocessed tip is easily depinned owing to its weak hydrophobicity. It has been optically confirmed that the nanoscale gas neck formed between a (relatively) hydrophilic tip and an interfacial nanobubble is more unstable than that formed by a (relatively) hydrophobic tip,[40] which is consistent with our results.

The hydrophilic tip does not dry easily, thus we assumed that the hydrophilic tip cannot penetrate the gas/liquid interface. Hence, the meniscus is not formed and a thin liquid film

always exists between the tip and the nanobubbles, as reported previously.[44,45] Therefore, the interaction between the hydrophilic tip and the nanobubble was observed to be the weakest and of the shortest duration among the three force curves. The weak attractive force experienced at a separation distance of 5 nm in the approach may result from the interaction from the substrate under the nanobubble. The hydrophilic tip compresses the nanobubbles without penetration. Therefore, it can be considered that the repulsive force results from the surface tension which acts to keep the deformed gas/liquid interface in a semispherical shape. In the retraction, the weak and short-range attractive force was evident around a separation distance of 10 nm. The weak attraction between the surface of the nanobubble and the hydrophilic tip has been reported in a prior simulation study.[56]

As mentioned before, the base radii of interfacial nanobubbles in the height images were less than those observed in the adhesion images, especially when scanned by the hydrophobic and unprocessed tips. To explain this, we assume that the turnaround point where the tip receives feedback is decided by the pinning position at the tip surface. Therefore, the degree of underestimation of the nanobubble profile is also determined by the pinning position. Pinning is derived from the chemical and geometrical conditions of the surface and can be therefore expected to work in the same manner in a scanning measurement. Thus, we consider a model where the penetration depth δ is constant on an interfacial nanobubble, as shown in Fig. 3. In the figure, r_{app} and h_{app} are the base radius and height of the nanobubbles measured in the height images, while r_{true} is the base radius of the nanobubbles estimated from the adhesion images. These three parameters can be obtained from the same set of scanning AFM data. In this model, the height of the undisturbed (true) nanobubble h_{true} can be described by

$$h_{true} = h_{app} + \delta. \tag{1}$$

We assume that the height of the positive meniscus formed at the tip surface can be ignored. Because the nanobubble shape is symmetrical with respect to the y-axis, the coordinate (x_{app}, y_{app}) of the apparent nanobubble is given as

$$x_{app}^2 + \{y_{app} + (R_{app} - h_{app})\}^2 = R_{app}^2, \tag{2}$$

where R_{app} is the radius of curvature of the interfacial nanobubble and is determined geometrically from r_{app} and the apparent contact angle. The equation that represents the true coordinate (x, y) of the nanobubble is obtained by translating the coordinates along the y-axis to a distance of δ, i.e.,

$$x^2 + \{y + (R_{app} - h_{app} - \delta)\}^2 = R_{app}^2. \tag{3}$$

By substituting the boundary conditions that $x = r_{true}$ and $y = 0$ into Eq. (3), δ is determined by

$$\delta = R_{app} - h_{app} - \sqrt{R_{app}^2 - r_{true}^2}. \tag{4}$$

The quantity h_{true} is also determined by substituting the calculated δ into Eq. (1). This model is applicable only for the hydrophobic tip, since pinning does not occur at the hydrophilic tip surface. Zhao *et al.* reported that the stiffness of an individual nanobubble is identical along the gas/water interface, based on an analysis of the nanobubbles' cross-sectional stiffness profiles obtained by the PF-QNM measurements.[14] In this study, therefore, we applied this model in the hydrophilic tip by assuming that the stiffness of the individual nanobubbles is almost constant everywhere and thus the depth at which the hydrophilic tip pushes the interface of the nanobubble is also constant.

In Fig. 4(a), the penetration depths δ obtained by the tips with different wettability are plotted against the true radius r_{true}. The penetration depths were unevenly distributed between 17 and 33, 8–19, and 0–1 nm for the hydrophobic, unprocessed, and hydrophilic tips, respectively. As the tip surfaces became more hydrophobic, the variance in the penetration depth increased. In addition, Fig. 4(a) shows no dependence of the penetration depth on r_{true}. Therefore, these results support our prediction that the penetration depth is determined not by the profile of the nanobubbles but by the nanoscale property of the tips, such as the wettability and structure. The plots also show that the penetration depth increased as the tips became hydrophobic. This is because the interaction between the tip surface and water molecules becomes weak as its hydrophobicity increases (i.e., the hydrophobic surface is easy to dry). In addition, the hydrophilic tip minimally pushed the gas/liquid interface and hardly caused any error. This is because the hydrophilic tip is repulsed by the surface tension from the thin liquid film, and can receive feedback immediately after the nanobubble is deformed.

The plot of h_{app} as a function of h_{true} is shown in Fig. 4(b). The plotted data acquired by each of the AFM tips are clearly seen to be linear relations. However, as the tip

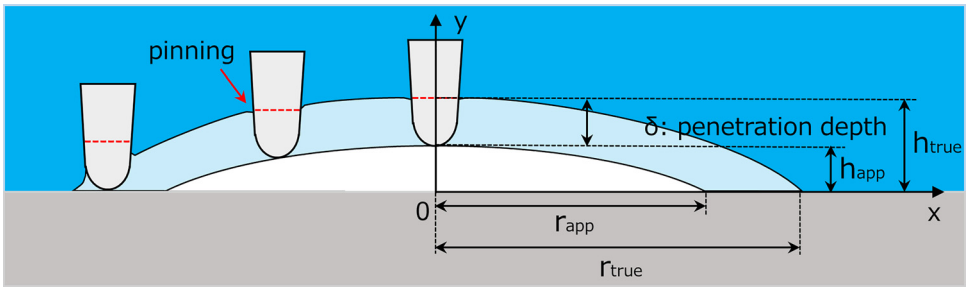

FIG. 3. Schematic diagram of the underestimation of the nanobubble profile. The pinning position at the surface of the tips determines the degree of underestimation.

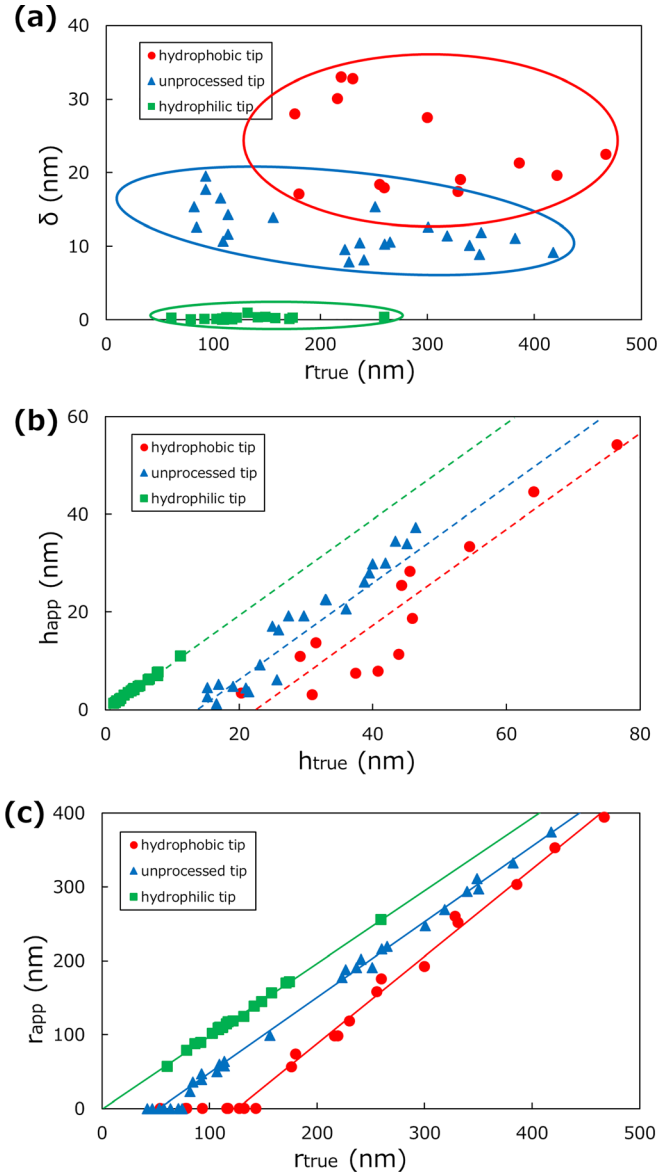

FIG. 4. (a) Penetration depth δ [calculated from Eq. (4)] scanned with the hydrophobic, unprocessed, and hydrophilic tips, and plotted as a function of r_{true}; (b) scatter plot of h_{true} [calculated from Eq. (1)] versus h_{app}; (c) r_{true} plotted versus r_{app}. The broken lines shown in (b) have a slope of 1.0. Linear regressions obtained by least-squares fitting are shown by the solid lines in (c). Since the true height cannot be estimated from nanobubbles whose apparent base radius is zero, they are not plotted in (b). The plots with zero apparent base radius value are not included in the linear regression estimations in (c).

surface became hydrophobic, the plots were distributed away from each of the broken lines with the slope of 1.0. This result shows that, although the penetration depth is determined by the properties of the tips, the reliability of the recalculated profile of interfacial nanobubbles decreases as the tips become more hydrophobic. In addition, the x-axis intercepts of the broken lines represent the minimal values of the nanobubble height which will be detected by the tips. The minimal values for the hydrophobic, unprocessed, and hydrophilic tips were 23, 14, and 0 nm, respectively. Therefore, the minimal values increased as the tips became hydrophobic. The surprising value of 0 nm indicates that a hydrophilic tip can detect the gas phase at the solid/liquid interface without underestimation. In contrast, the values obtained by the unprocessed and hydrophobic tips demonstrate that a hydrophobic tip may fail to detect small nanobubbles.

The relation between r_{app} and r_{true} is shown in Fig. 4(c). As the tips became more hydrophobic, the difference between r_{app} and r_{true}, namely the underestimation of the base radius, increased. This is because the tip with stronger hydrophobicity can easily reach the substrate surface under the nanobubbles owing to the long penetration depth. The slopes of the regression lines increased slightly as the wettability approached hydrophobic (1.00, 1.02, and 1.18, respectively, for the hydrophilic, unprocessed, and hydrophilic tips). This result suggests that the degree of underestimation of the base radii of large nanobubbles was less than that of the small nanobubbles when measured using a hydrophobic tip. This observation can be explained by considering the dependence of the contact angle on the base radius. It has been reported that the contact angle of interfacial nanobubbles decreases as their base radius increases.[16,31,34,49] As the contact angle decreases, the slope of a height-versus-base radius plot increases. Thus, because the AFM tip penetrates the gas/liquid interface at a constant depth, the underestimation of the base radius of larger nanobubbles decreases. The minimal values of the base radius represented by the x-axis intercepts of the regression lines were 126, 53, and 0 nm, corresponding to the data collected with the hydrophobic, unprocessed, and hydrophilic tips, respectively. The minimal values are in good agreement with the values measured at zero apparent base radius. This result shows that the nanoscale gas domain can be accurately measured using a hydrophilic AFM tip, while a hydrophobic tip cannot accurately measure small nanobubbles, consistent with the result obtained from Fig. 4(b).

In our model, we do not take the AFM tip broadening into account. Tip broadening will influence the true base radius r_{true} and thus normally needs to be considered. However, in this study, we examine the influence of AFM tips on the nanobubble profile on the basis of the pinning position. The pinning position depends not only on AFM tip broadening but also on wettability and surface roughness. In scans using a hydrophobic tip, the influences of wettability and surface roughness are stronger than that of AFM tip broadening, thus we ignored the AFM tip broadening in these measurements. For scans with a hydrophilic tip, the AFM tip broadening should be considered because a hydrophilic tip does not penetrate the gas/liquid interface and pinning does not occur. The correction based on AFM tip broadening has been discussed in previous reports.[10,11]

From these results, the profiles of the interfacial nanobubbles obtained by hydrophobic and unprocessed tips in the PFT mode need to be recalculated using the data of the nanomechanical mapping. However, the reliability of the recalculated profile based on the data obtained using hydrophobic tips decreases because the error in penetration depth increases. In addition, nanobubbles smaller than the minimal profiles cannot be detected and recalculated as height data. In contrast, it is clear from the present study that the hydrophilic tip is most suitable to image the shape of the

interfacial nanobubbles with no underestimation and perfect detection. It has been reported that the profiles of interfacial nanobubbles obtained using a hydrophilic tip in the tapping mode need to be corrected by an extrapolation method,[44,45] but it can be considered that the profiles obtained by a hydrophilic tip with a low peak force setpoint in the PFT mode do not need such correction. Furthermore, we emphasize that a correction based on the broadening of the AFM tip, as has been suggested elsewhere,[10,11] should not be applied to the nanobubble profiles in a height image obtained using a hydrophobic tip, because this correction can only be used under the condition that the tip does not penetrate (or deform) the nanobubble interface. Conversely, application of the correction to the profile obtained by a hydrophilic tip will lead to a more exact profile. These results will ensure the reliability of bubble shape measurements obtained with hydrophilic AFM tips in the PFT mode that have been reported so far. The present results should prove important for the detection of nanobubbles of all sizes and for the construction of reliable theories for interfacial nanobubbles.

CONCLUSIONS

We obtained AFM height and adhesion images and force curves of nanobubbles at an HOPG/water interface, using the PFT mode and AFM tips treated to be hydrophobic, hydrophilic, and of intermediate wettability. By analyzing the force curves, we attributed the repulsive force acting on the hydrophobic and unprocessed tips during the measurements to the positive meniscus derived from contact line pinning at the tip surface, while the repulsive force experienced by the hydrophilic tip was generated by the restoration of the deformed gas/liquid interface to a semispherical shape. Therefore, the AFM feedback mechanism varies with the tip wettability. Next, we quantitatively estimated the depth upto which each of the tips penetrated (or deformed) the surface of the nanobubbles and constructed the true profiles of the nanobubbles using the height and adhesion data. As a result, the underestimation of the nanobubble profile clearly depended on the wettability of the tips. The hydrophobic and unprocessed tips penetrated the gas/liquid interface and inevitably underestimated the height and base radius of the nanobubbles. In contrast, the hydrophilic tip almost never pushed the surface of the nanobubbles and could characterize the profiles of nanobubbles of any size without underestimation. Thus, AFM measurements using a hydrophilic tip in the PFT mode were found to be the most suitable approach to characterize interfacial nanobubbles.

SUPPLEMENTARY MATERIAL

See supplementary material for the details with regard to the confirmation that Teflon film was smoothly coated on the AFM tip surface and the discrimination between the interfacial nanobubbles and contaminant nanodroplets.

ACKNOWLEDGMENTS

This work was partially supported by JSPS KAKENHI Grant Nos. JP16H02315, JP16H04280, JP16K06126, JP16K14174, and JP17H03186. PF-QNM measurements were performed at the Center of Advanced Instrumental Analysis, Kyushu University.

[1]Y. Gao, J. Li, H. C. Shum, and H. Chen, Langmuir **32**, 4815 (2016).
[2]S. Yang and A. Duisterwinkel, Langmuir **27**, 11430 (2011).
[3]Y. Nam and Y. S. Ju, Appl. Phys. Lett. **93**, 103115 (2008).
[4]L. Gao, G. X. Ni, Y. Liu, B. Liu, A. H. Castro Neto, and K. P. Loh, Nature **505**, 190 (2014).
[5]S.-T. Lou, Z.-Q. Ouyang, Y. Zhang, X.-J. Li, J. Hu, M.-Q. Li, and F.-J. Yang, J. Vac. Sci. Technol. B **18**, 2573 (2000).
[6]J. Yang, J. Duan, D. Fornasiero, and J. Ralston, J. Phys. Chem. B **107**, 6139 (2003).
[7]A. C. Simonsen, P. L. Hansen, and B. Klösgen, J. Colloid Interface Sci. **273**, 291 (2004).
[8]X. H. Zhang, X. D. Zhang, S. T. Lou, Z. X. Zhang, J. L. Sun, and J. Hu, Langmuir **20**, 3813 (2004).
[9]S. Yang, S. M. Dammer, N. Bremond, H. J. W. Zandvliet, E. S. Kooij, and D. Lohse, Langmuir **23**, 7072 (2007).
[10]B. M. Borkent, S. De Beer, F. Mugele, and D. Lohse, Langmuir **26**, 260 (2010).
[11]B. Song, W. Walczyk, and H. Schönherr, Langmuir **27**, 8223 (2011).
[12]X. Zhang, M. H. Uddin, H. Yang, G. Toikka, W. Ducker, and N. Maeda, Langmuir **28**, 10471 (2012).
[13]W. Walczyk, P. M. Schön, and H. Schönherr, J. Phys. Condens. Matter **25**, 184005 (2013).
[14]B. Zhao, Y. Song, S. Wang, B. Dai, L. Zhang, Y. Dong, J. Lü, and J. Hu, Soft Matter **9**, 8837 (2013).
[15]X. Wang, B. Zhao, J. Hu, S. Wang, R. Tai, X. Gao, and L. Zhang, Phys. Chem. Chem. Phys. **19**, 1108 (2016).
[16]H. Teshima, T. Nishiyama, and K. Takahashi, J. Chem. Phys. **146**, 14708 (2017).
[17]H. An, B. H. Tan, and C.-D. Ohl, Langmuir **32**, 12710 (2016).
[18]B. Song, K. Chen, M. Schmittel, and H. Schönherr, Langmuir **32**, 11172 (2016).
[19]H. C. Ko, W. H. Hsu, C. W. Yang, C. K. Fang, Y. H. Lu, and I. S. Hwang, Langmuir **32**, 11164 (2016).
[20]X. H. Zhang, A. Quinn, and W. A. Ducker, Langmuir **24**, 4756 (2008).
[21]X. Zhang, D. Y. C. Chan, D. Wang, and N. Maeda, Langmuir **29**, 1017 (2013).
[22]S. R. German, X. Wu, H. An, V. S. J. Craig, T. L. Mega, X. Zhang, R. Corporation, U. States, B. Engineering, A. Mathematics, P. Sciences, and C. Act, ACS Nano **8**, 6193 (2014).
[23]T. Nishiyama, K. Takahashi, T. Ikuta, Y. Yamada, and Y. Takata, ChemPhysChem **17**, 1500 (2016).
[24]P. S. Epstein and M. S. Plesset, J. Chem. Phys. **18**, 1505 (1950).
[25]S. Ljunggren and J. C. Eriksson, Colloids Surf. A **129–130**, 151 (1997).
[26]W. A. Ducker, Langmuir **25**, 8907 (2009).
[27]K. Yasui, T. Tuziuti, W. Kanematsu, and K. Kato, Phys. Rev. E **91**, 33008 (2015).
[28]M. P. Brenner and D. Lohse, Phys. Rev. Lett. **101**, 214505 (2008).
[29]J. R. T. Seddon, H. J. W. Zandvliet, and D. Lohse, Phys. Rev. Lett. **107**, 2 (2011).
[30]Y. Liu and X. Zhang, J. Chem. Phys. **141**, 134702 (2014).
[31]D. Lohse and X. Zhang, Phys. Rev. E **91**, 31003 (2015).
[32]J. H. Weijs and D. Lohse, Phys. Rev. Lett. **110**, 1 (2013).
[33]N. Kameda, N. Sogoshi, and S. Nakabayashi, Surf. Sci. **602**, 1579 (2008).
[34]N. Kameda and S. Nakabayashi, Chem. Phys. Lett. **461**, 122 (2008).
[35]N. D. Petsev, M. S. Shell, and L. G. Leal, Phys. Rev. E **88**, 10402 (2013).
[36]D. Shin, J. B. Park, Y. J. Kim, S. J. Kim, J. H. Kang, B. Lee, S. P. Cho, B. H. Hong, and K. S. Novoselov, Nat. Commun. **6**, 6068 (2015).
[37]S.-Y. Liu, P. Kundu, T.-W. Huang, Y.-J. Chuang, F.-G. Tseng, Y. Lu, M.-L. Sui, and F.-R. Chen, Nano Energy **31**, 218 (2017).
[38]Y. Tomo, K. Takahashi, T. Nishiyama, T. Ikuta, and Y. Takata, Int. J. Heat Mass Transfer **108**, 1460 (2017).
[39]C. U. Chan and C. D. Ohl, Phys. Rev. Lett. **109**, 1 (2012).
[40]B. H. Tan, H. An, and C.-D. Ohl, Phys. Rev. Lett. **118**, 54501 (2017).
[41]T. Nishiyama, Y. Yamada, T. Ikuta, K. Takahashi, and Y. Takata, Langmuir **31**, 982 (2015).
[42]N. Ishida, T. Inoue, M. Miyahara, and K. Higashitani, Langmuir **16**, 6377 (2000).

[43]W. Walczyk and H. Schönherr, Langmuir **29**, 620 (2013).
[44]W. Walczyk and H. Schönherr, Langmuir **30**, 7112 (2014).
[45]W. Walczyk and H. Schönherr, Langmuir **30**, 11955 (2014).
[46]L. Wang, X. Wang, L. Wang, J. Hu, C. L. Wang, B. Zhao, X. Zhang, R. Tai, M. He, L. Chen, and L. Zhang, Nanoscale **9**, 1078 (2017).
[47]Y. Wang, X. Li, S. Ren, H. Tedros Alem, L. Yang, and D. Lohse, Soft Matter **13**, 5381 (2017).
[48]C. U. Chan, M. Arora, and C. D. Ohl, Langmuir **31**, 7041 (2015).
[49]C. Xu, S. Peng, G. G. Qiao, V. Gutowski, D. Lohse, and X. Zhang, Soft Matter **10**, 7857 (2014).
[50]L. Zhang, X. Zhang, Y. Zhang, J. Hu, and H. Fang, Soft Matter **6**, 4515 (2010).
[51]X. H. Zhang, N. Maeda, and J. Hu, J. Phys. Chem. B **112**, 13671 (2008).
[52]S. Yang, E. S. Kooij, B. Poelsema, D. Lohse, and H. J. W. Zandvliet, Europhys. Lett. **81**, 64006 (2008).
[53]R. P. Berkelaar, E. Dietrich, G. a M. Kip, E. S. Kooij, H. J. W. Zandvliet, and D. Lohse, Soft Matter **10**, 4947 (2014).
[54]D. Seo, S. R. German, T. L. Mega, and W. A. Ducker, J. Phys. Chem. C **119**, 14262 (2015).
[55]N. Hain, D. Wesner, S. I. Druzhinin, and H. Schönherr, Langmuir **32**, 11155 (2016).
[56]Z. Guo, Y. Liu, Q. Xiao, H. Schönherr, and X. Zhang, Langmuir **32**, 751 (2016).